The Role of Polarons in Water Splitting: the Case of $BiVO_4$

Julia Wiktor,* Francesco Ambrosio, and Alfredo Pasquarello

Chaire de Simulation à l'Echelle Atomique (CSEA), Ecole Polytechnique Fédérale de Lausanne (EPFL), CH-1015 Lausanne, Switzerland

E-mail: julia.wiktor@epfl.ch

*To whom correspondence should be addressed

Abstract

We study hole and electron polarons in $BiVO_4$ at finite temperature through hybrid functional molecular dynamics simulations. Through the thermodynamic integration method, we obtain the transition levels corresponding to the localized charges at 300 K. We observe that the polaron levels achieved in this way lie significantly closer to each other than at 0 K. We find both hole and electron levels to lie within the band gap, with binding energies of 0.11 and 0.88 eV, respectively. Our calculations show that the polaron localization significantly affects the alignment at the solid/liquid interface and that electron-hole recombination through polaronic states competes with the evolution of the water-splitting reaction in $BiVO_4$.

Graphical TOC Entry

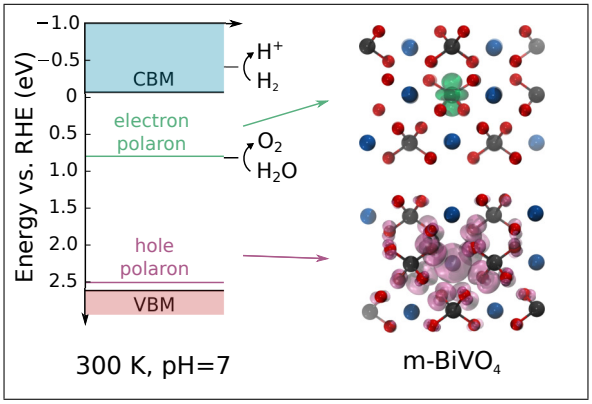

Photocatalytic water splitting is a promising way of generating chemical fuels from solar energy.[1–3] To achieve higher efficiency of photoelectrochemical cells, the search for new functional materials with optimal properties is ongoing. Several high throughput studies have recently been undertaken and resulted in the proposal of several ternary metal-oxide semiconductors as suitable absorber candidates.[4–7] Since these findings inspire considerable experimental effort, it is of great importance to verify the usefulness of the considered descriptors. In the computational screening of photoabsorbers for water splitting, two requirements are generally considered. First, the band gap of the semiconductor has to be larger than at least 1.23 eV, which is the energy per transferred electron needed to split water. Accounting for losses at the semiconductor-liquid junction, due to e.g. overpotentials, the minimal value should rather be 1.6–2.4 eV.[8,9] Second, for single absorber photoelectrochemical devices, the redox potentials of water should be straddled by the valence band maximum (VBM) and conduction band minimum (CBM) of the semiconductor.[3,10] This is based on the assumption that the H^+ reduction and H_2O oxidation are driven by delocalized holes and electrons occupying the highest and lowest levels of the valence and conduction band, respectively.

It has been shown for many metal oxides that excess charges induce lattice distortion and form localized polarons.[11–17] If stable, such quasiparticles, occupy energy levels within the gap. Therefore, upon their creation within the semiconductor, the charge carriers diffuse through the lattice by hopping from one stable position to another, until they recombine, get trapped, or reach the solid/liquid interface. Besides inhibiting carrier transport kinetics, the formation of polarons might also impact the catalysis process at the interface. Since the water-splitting reaction is driven by photogenerated excess charges, the reaction can only occur if the redox levels are not only straddled by the band edges, but also by the polaron levels. This is in contrast with the previously described screening methodologies for metal oxide photoabsorbers, and might prove a crucial factor in future material discovery efforts.

Monoclinic bismuth vanadate (m-$BiVO_4$) has been considered as a promising photoanode for water-splitting photoelectrochemical cells[18–21] and has thus been extensively studied

both experimentally and computationally. Since $BiVO_4$ is representative of a broader class of complex metal oxides,[22] it can be used as a benchmark material to understand crucial phenomena affecting the water-splitting reaction. Additionally, polarons in $BiVO_4$ have already been observed.[16,17,23–27] However, previous theoretical studies only considered charge localization at 0 K, while the electronic structure of $BiVO_4$ is strongly affected by thermal distortions.[28] Additionally, the thermodynamic transition levels of polarons in this material have not been addressed so far.

In this Letter, we highlight the effect of polaronic energy levels on water splitting by applying state-of-the-art computational methods. To achieve a realistic description of the localization of excess holes and electrons in $BiVO_4$, we perform hybrid functional molecular dynamics (MD) simulations. We determine the polaron binding energies at finite temperature through the thermodynamic integration method, which is suitable for calculating free-energy differences. Finally, we align the polaronic levels with the redox potentials of water and discuss the consequences of this alignment on the water-splitting reaction.

Since standard semilocal functionals are not able to treat the self-interaction error[29–31] and erroneously favor the delocalization of electronic states, we study the polarons with the hybrid functional PBE0.[32] We set the α parameter to 0.22, as this value leads to a fundamental band gap in agreement with experiment (about 2.6 eV), after including all relevant corrections.[28] The MD simulations are performed with the CP2K code[33] in the canonical NVT ensemble at a temperature of 300 K. The orbitals are described with atom-centered Gaussian-type basis functions and the electron density is re-expanded with an auxiliary plane-wave basis set. We use the MOLOPT basis set[34] for Bi, O, and V, and a cutoff of 600 Ha for the plane waves. Core-valence interactions are described by Goedecker-Teter-Hutter pseudopotentials.[35] The calculations are carried out for an optimized orthorhombic supercell containing 192 atoms (a = 10.30, b = 10.26, and c = 23.50 Å) and the Brillouin zone is sampled at the Γ point. The time step is set to 1 fs and the simulations are carried out for 5–10 ps. We study hole and electron polarons, by removing or adding one electron to

the supercell. In this case we perform spin-polarized calculations. Since the CP2K code does not include spin-orbit effects and only allows for Γ-point sampling of the Brillouin zone, we correct the positions of the band edges of $BiVO_4$ using the results of Ref. 28. We neglect finite-size corrections in the calculations,[36] due to the high dielectric constant of $BiVO_4$ (ϵ_0=68).[37]

To obtain the energy levels of the hole and electron polarons, we follow the grand-canonical formulation for defects in crystalline materials.[36,38] In this case, the charge transition level μ can be written as:

$$\mu(q/q') = \frac{G^q[X] - G^{q'}[X]}{q' - q} - \epsilon_{\mathrm{v}}, \tag{1}$$

where $G^q[X]$ and $G^{q'}[X]$ are the free energies of the defect X in the charge states q and q', and ϵ_{v} is the position of the valence band maximum. To take into account the thermal disorder, we calculate free-energy differences with the thermodynamic integration method.[39] In the following, we neglect volume changes and apply the linear Marcus approximation. The hole polaron level can then be calculated as:[40]

$$\mu(\mathrm{h_{loc}}) = \frac{\langle \Delta E_{\mathrm{h}} \rangle_0 + \langle \Delta E_{\mathrm{h}} \rangle_1}{2} - \epsilon_{\mathrm{v}}, \tag{2}$$

where $\langle \Delta E_{\mathrm{h}} \rangle_0$ is the energy of vertical removal of one electron in the bulk configuration and $\langle \Delta E_{\mathrm{h}} \rangle_1$ is the energy of adding an electron in the geometry of the hole polaron. In the case of the electron, the transition level reads:

$$\mu(\mathrm{el_{loc}}) = \frac{\langle \Delta E_{\mathrm{el}} \rangle_0 + \langle \Delta E_{\mathrm{el}} \rangle_1}{2} - \epsilon_{\mathrm{v}}, \tag{3}$$

where $\langle \Delta E_{\mathrm{el}} \rangle_0$ corresponds to the vertical injection of one electron in the bulk geometry and $\langle \Delta E_{\mathrm{el}} \rangle_1$ to the removal of an electron in the polaron geometry. In the case of the electron, for which the energy differences are larger, we examine the validity of the linear Marcus

approximation by including an additional value of the Kirkwood coupling parameter[39,41] at 0.5. The additional point changes the position of the electron polaron transition level by only 0.07 eV.

First, we study the electron and hole polarons at 0 K. The charge localization is given in Fig. 1. The charge distribution is consistent with previous studies.[24,25] The electron polaron localizes around a vanadium atom, which changes its ionization state from +5 to +4. At the same time, the V–O bond lengths around the polaron increase, from about 1.72 Å to 1.81 Å. The localized polaron introduces a one-particle level within the band gap at 1.43 eV below the conduction band minimum. Through Eq. (1), we find that the associated transition level lies at 1.09 eV below the CBM.

The hole polaron is mostly distributed between one bismuth and eight oxygen atoms. The charge localization results in Bi–O bond shortening, from about 2.48 Å on average to about 2.42 Å. The charge occupies a one-particle level at 0.78 eV above the valence band maximum. Through Eq. (1), we obtain a transition level at 0.30 eV above VBM. We give the alignment of the polaronic transition levels with the band edges of $BiVO_4$ in Fig. 2. We note that the fundamental (electronic) band gap at 0 K amounts to 3.61 eV when calculated with the current setup. This results in a band gap of 2.69 eV after including thermal and quantum renormalization effects.[28]

In Ref. 28, we have observed that the electronic structure of $BiVO_4$ is strongly affected by thermal disorder. We also expect the temperature to have an effect on the polaronic energy levels. Therefore, we determine the polaronic energy levels through thermodynamic integration based on hybrid functional molecular dynamics. First, we study the evolution of the electron polaron. We observe that during a MD duration of 5 ps, the electron remains localized around the same vanadium atom. Also the geometry around the V^{4+} ion does not change, as the average V–O bond length still amounts to 1.81 Å. Through thermodynamic integration at 300 K, we obtain a transition level at 0.88 eV below the CBM, as illustrated in Fig. 2. The binding energy of the electron polaron (energy separation from the CBM)

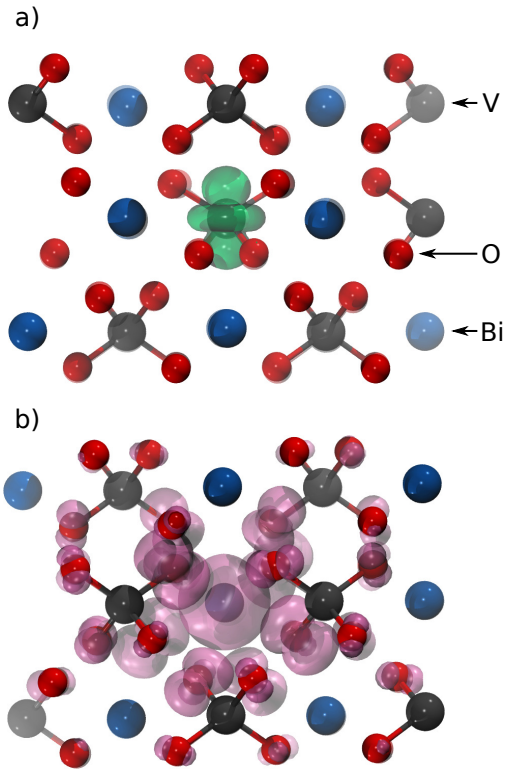

Figure 1: Isodensities of the (a) electron and (b) hole polarons in monoclinic $BiVO_4$ at 0 K. The electron is localized around a vanadium atom and the hole around a bismuth atom.

reduces by 0.21 eV due to temperature, while the absolute position of the transition level shifts by 0.16 eV towards lower energies.

For the hole polaron, we carry out molecular dynamics lasting for 10 ps. Since the hole polaron is much less localized than the electron, we observe polaron hopping and the charge localizes around various bismuth atoms during the simulation. Most of the time the charge is distributed between one bismuth and eight oxygen atoms. In about 20% of the configurations, we observe a stronger localization of the hole, mostly at a single oxygen atom. From the thermodynamic integration, we obtain a transition level lying at 0.11 eV above the valence band maximum, consistent with the weaker charge localization compared to the electron polaron. We note that the calculated binding energy of the hole polaron at 300 K is close to the thermal hopping activation energy of about 0.09 eV, derived from THz spectroscopy measurements.[16] The different localization of the hole and the electron polaron

is consistent with the observation that the electron mobility limits the photocarrier transport and extraction in $BiVO_4$.[42–45] The relatively weak localization of the hole polaron is also in line with the study of Butler *et al.*,[17] who observed that above a critical Mott concentration, the wavefunction of trapped positive charges can overlap leading to an enhanced charge mobility. We note that the binding energy of the hole at 300 K is lower than the one calculated at 0 K by 0.30 eV, similarly to the case of the electron polaron. Further, we observe that at 300 K the polaronic energy levels also differ from the 0 K case on an absolute energy scale (see Fig. 2).

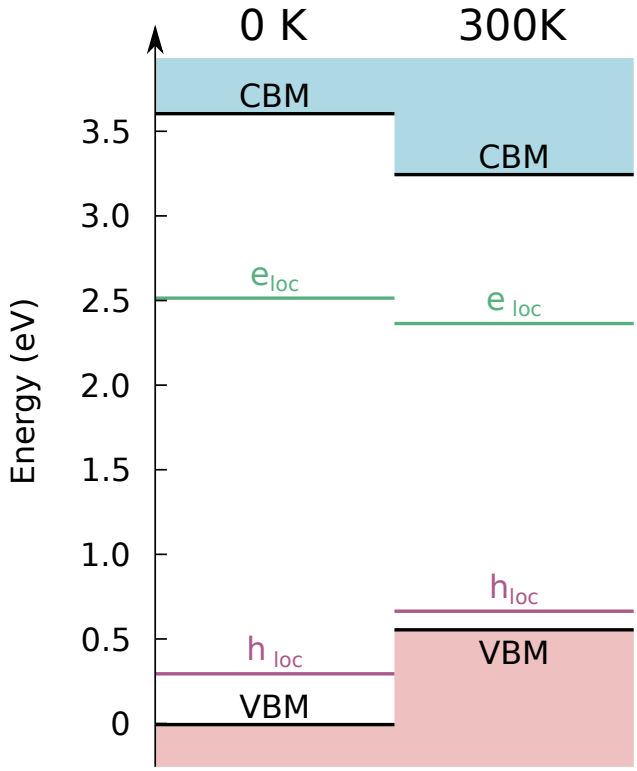

Figure 2: Energy diagram showing the transition levels of the hole and electron polarons with respect to the band edges of $BiVO_4$ at 0 and 300 K. The results are aligned through the V 3*s* level.

Next, we consider the effect of the energy levels of the electron and hole polarons on the water-splitting reaction. First, we observe that the energy separation between the localized charge carriers amounts to 1.70 eV. This is smaller by about 1 eV than the fundamental band gap of 2.69 eV. This considerable difference shows how drastic of an effect the localization of

charge carriers can have on the alignment of the energy levels in this class of materials. The significant difference between the energy levels of delocalized and localized states highlighted here could have a critical impact on the search for new materials among metal oxides.

In Fig. 3 we align the band edges and the polaronic levels with the H^+/H_2 and H_2O/O_2 redox levels. The alignment of these levels is illustrated for pH = 7. For this purpose, we use the pH of zero point charge of $BiVO_4$ calculated in Ref. 46 and the band alignment at the $BiVO_4$/water interface given in Ref. 47. We note that, as the same pH-dependence (Nernstian behavior) is expected for all the presented levels, the relative positions of the various levels will be preserved at other pH.

The hole polaron in $BiVO_4$ is relatively weakly localized, and hence the H_2O/O_2 redox level is positioned above both the VBM and the polaron level. However, the electron polaron level falls very close to the H_2O/O_2 redox level. This means that the recombination process between electron and hole polarons at the $BiVO_4$/water interface could compete with the charge transfer to the electrolyte. This observation is in agreement with experimental findings showing that the photocurrent of $BiVO_4$ is limited by surface recombination processes.[48] We note that the binding energies of the polarons are expected to increase near the surface, which would imply an even stronger tendency towards recombination.

Polaron levels as calculated in the present work would also severely restrict the scope of band level engineering efforts. The H^+/H_2 potential is found at 0.34 eV above the CBM, which suggests that the band edge could reach this level through band structure engineering, and that slightly modified monoclinic $BiVO_4$ could be suitable for driving overall water splitting. However, considering that the localized electron lies at 1.22 eV below the redox potential, water reduction would be much more difficult to achieve. This is consistent with the fact that the overall water-splitting reaction based on $BiVO_4$ could only be achieved through strong modification of its structure or composition by alloying.[49,50] The points mentioned above suggest that a reevaluation of the descriptors used in materials screening processes might be in order to account for charge localization in metal oxides.

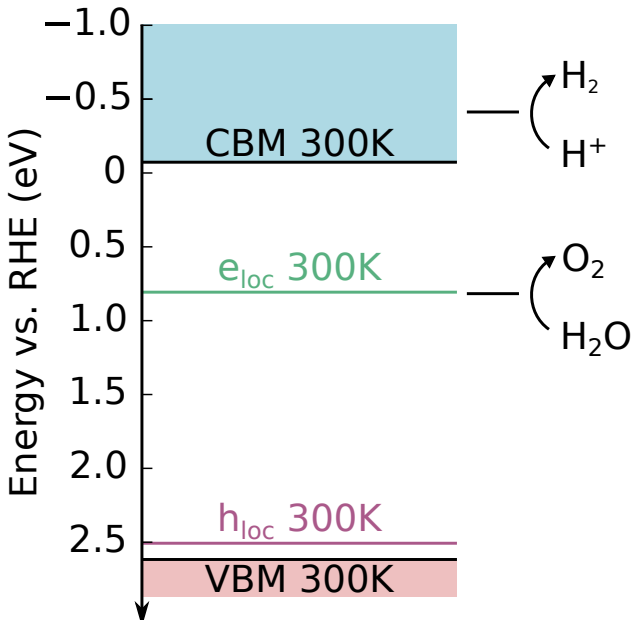

Figure 3: Alignment of the band edges of $BiVO_4$ and polaron transition levels at 300 K with H^+/H_2 and O_2/H_2O redox levels at pH = 7.

In conclusion, we highlighted the role of hole and electron polarons in $BiVO_4$ at finite temperature by combining the thermodynamic integration method and hybrid functional molecular dynamics simulations. The polaron levels calculated at 300 K lie significantly closer to each other than at 0 K. We found that the localization of both the hole and the electron introduce levels within the band gap, with binding energies of 0.11 eV and 0.88 eV, respectively. The polaron localization significantly affects the alignment at the $BiVO_4$/water interface, suggesting that electron-hole recombination through polaronic states could hamper the evolution of the water-splitting reaction.

Acknowledgement

The authors acknowledge the financial support from the Swiss National Science Foundation (SNSF) (Grant No. 200020-172524). This work has been realized in relation to the National Center of Competence in Research (NCCR) "Materials' Revolution: Computational Design and Discovery of Novel Materials (MARVEL)" of the SNSF. We used computational resources

of CSCS and SCITAS-EPFL.

Supporting Information Available

Sample CP2K input file used to study the electron polaron in $BiVO_4$ at 0 K.

References

(1) Fujishima, A.; Honda, K. Electrochemical Photolysis of Water at a Semiconductor Electrode. *Nature* **1972**, *238*, 37–38.

(2) Maeda, K.; Teramura, K.; Lu, D.; Takata, T.; Saito, N.; Inoue, Y.; Domen, K. Photocatalyst Releasing Hydrogen from Water. *Nature* **2006**, *440*, 295–295.

(3) Walter, M. G.; Warren, E. L.; McKone, J. R.; Boettcher, S. W.; Mi, Q.; Santori, E. A.; Lewis, N. S. Solar Water Splitting Cells. *Chem. Rev.* **2010**, *110*, 6446.

(4) Katz, J. E.; Gingrich, T. R.; Santori, E. A.; Lewis, N. S. Combinatorial Synthesis and High-Throughput Photopotential and Photocurrent Screening of Mixed-Metal Oxides for Photoelectrochemical Water Splitting. *Energy Env. Sci.* **2009**, *2*, 103–112.

(5) Wu, Y.; Lazic, P.; Hautier, G.; Persson, K.; Ceder, G. First Principles High Throughput Screening of Oxynitrides for Water-Splitting Photocatalysts. *Energy Environ. Sci.* **2013**, *6*, 157–168.

(6) Zhou, L.; Yan, Q.; Shinde, A.; Guevarra, D.; Newhouse, P. F.; Becerra-Stasiewicz, N.; Chatman, S. M.; Haber, J. A.; Neaton, J. B.; Gregoire, J. M. High Throughput Discovery of Solar Fuels Photoanodes in the CuO–V_2O_5 System. *Adv. Energy Mater.* **2015**, *5*, 1500968.

(7) Yan, Q.; Yu, J.; Suram, S. K.; Zhou, L.; Shinde, A.; Newhouse, P. F.; Chen, W.; Li, G.; Persson, K. A.; Gregoire, J. M. et al. Solar Fuels Photoanode Materials Discovery by

Integrating High-Throughput Theory and Experiment. *Proc. Natl. Acad. Sci.* **2017**, *114*, 3040–3043.

(8) Bolton, J. R.; Strickler, S. J.; Connolly, J. S. Limiting and Realizable Efficiencies of Solar Photolysis of Water. *Nature* **1985**, *316*, 495–500.

(9) Turner, J. A. A Realizable Renewable Energy Future. *Science* **1999**, *285*, 687–689.

(10) Nørskov, J. K.; Bligaard, T.; Rossmeisl, J.; Christensen, C. H. Towards the Computational Design of Solid Catalysts. *Nat. Chem.* **2009**, *1*, 37.

(11) Di Valentin, C.; Selloni, A. Bulk and Surface Polarons in Photoexcited Anatase TiO_2. *J. Phys. Chem. Lett.* **2011**, *2*, 2223.

(12) Setvin, M.; Franchini, C.; Hao, X.; Schmid, M.; Janotti, A.; Kaltak, M.; Van de Walle, C. G.; Kresse, G.; Diebold, U. Direct View at Excess Electrons in TiO_2 Rutile and Anatase. *Phys. Rev. Lett.* **2014**, *113*, 086402.

(13) Janotti, A.; Varley, J. B.; Choi, M.; Van de Walle, C. G. Vacancies and Small Polarons in $SrTiO_3$. *Phys. Rev. B* **2014**, *90*, 085202.

(14) Bjaalie, L.; Janotti, A.; Krishnaswamy, K.; Van de Walle, C. G. Point Defects, Impurities, and Small Hole Polarons in $GdTiO_3$. *Phys. Rev. B* **2016**, *93*, 115316.

(15) Rettie, A. J.; Chemelewski, W. D.; Emin, D.; Mullins, C. B. Unravelling Small-Polaron Transport in Metal Oxide Photoelectrodes. *J. Phys. Chem. Lett.* **2016**, *7*, 471–479.

(16) Ziwritsch, M.; Müller, S.; Hempel, H.; Unold, T.; Abdi, F. F.; van de Krol, R.; Friedrich, D.; Eichberger, R. Direct Time-Resolved Observation of Carrier Trapping and Polaron Conductivity in $BiVO_4$. *ACS Energy Lett.* **2016**, *1*, 888–894.

(17) Butler, K.; Dringoli, B.; Zhou, L.; Rao, P.; Walsh, A.; Titova, L. Ultrafast Carrier Dynamics in $BiVO_4$ Thin Film Photoanode Material: Interplay Between Free Carriers,

Trapped Carriers and Low-Frequency Lattice Vibrations. *J. Mater. Chem. A* **2016**, *4*, 18516–18523.

(18) Kudo, A.; Omori, K.; Kato, H. A Novel Aqueous Process for Preparation of Crystal Form-Controlled and Highly Crystalline $BiVO_4$ Powder from Layered Vanadates at Room Temperature and Its Photocatalytic and Photophysical Properties. *J. Am. Chem. Soc.* **1999**, *121*, 11459–11467.

(19) Yu, J.; Kudo, A. Effects of Structural Variation on the Photocatalytic Performance of Hydrothermally Synthesized $BiVO_4$. *Advanced Functional Materials* **2006**, *16*, 2163–2169.

(20) Luo, H.; Mueller, A. H.; McCleskey, T. M.; Burrell, A. K.; Bauer, E.; Jia, Q. Structural and Photoelectrochemical Properties of $BiVO_4$ Thin Films. *J. Phys. Chem. C* **2008**, *112*, 6099–6102.

(21) Park, Y.; McDonald, K. J.; Choi, K.-S. Progress in Bismuth Vanadate Photoanodes for Use in Solar Water Oxidation. *Chem. Soc. Rev.* **2013**, *42*, 2321–2337.

(22) Sharp, I. D.; Cooper, J. K.; Toma, F. M.; Buonsanti, R. Bismuth Vanadate As a Platform for Accelerating Discovery and Development of Complex Transition-Metal Oxide Photoanodes. *ACS Energy Lett.* **2016**, *2*, 139–150.

(23) Kweon, K. E.; Hwang, G. S. Surface Structure and Hole Localization in Bismuth Vanadate: A First Principles Study. *Appl. Phys. Lett.* **2013**, *103*, 131603.

(24) Kweon, K. E.; Hwang, G. S. Structural Phase-Dependent Hole Localization and Transport in Bismuth Vanadate. *Phys. Rev. B* **2013**, *87*, 205202.

(25) Kweon, K. E.; Hwang, G. S.; Kim, J.; Kim, S.; Kim, S. Electron Small Polarons and Their Transport in Bismuth Vanadate: A First Principles Study. *Phys. Chem. Chem. Phys.* **2015**, *17*, 256–260.

(26) Liu, T.; Zhou, X.; Dupuis, M.; Li, C. The Nature of Photogenerated Charge Separation Among Different Crystal Facets of $BiVO_4$ Studied by Density Functional Theory. *Phys. Chem. Chem. Phys.* **2015**, *17*, 23503–23510.

(27) Rettie, A. J.; Chemelewski, W. D.; Lindemuth, J.; McCloy, J. S.; Marshall, L. G.; Zhou, J.; Emin, D.; Mullins, C. B. Anisotropic Small-Polaron Hopping in W: $BiVO_4$ Single Crystals. *Appl. Phys. Lett.* **2015**, *106*, 022106.

(28) Wiktor, J.; Reshetnyak, I.; Ambrosio, F.; Pasquarello, A. Comprehensive Modeling of the Band Gap and Absorption Spectrum of $BiVO_4$. *Phys. Rev. Mater.* **2017**, *1*, 022401.

(29) Zhang, Y.; Yang, W. A Challenge for Density Functionals: Self-Interaction Error Increases for Systems with a Noninteger Number of Electrons. *J. Chem. Phys.* **1998**, *109*, 2604–2608.

(30) Pacchioni, G.; Frigoli, F.; Ricci, D.; Weil, J. A. Theoretical Description of Hole Localization in a Quartz al Center: The Importance of Exact Electron Exchange. *Phys. Rev. B* **2000**, *63*, 054102.

(31) Lægsgaard, J.; Stokbro, K. Hole Trapping at Al Impurities in Silica: A Challenge for Density Functional Theories. *Phys. Rev. Lett.* **2001**, *86*, 2834.

(32) Perdew, J. P.; Ernzerhof, M.; Burke, K. Rationale for Mixing Exact Exchange with Density Functional Approximations. *J. Chem. Phys.* **1996**, *105*, 9982–9985.

(33) VandeVondele, J.; Krack, M.; Mohamed, F.; Parrinello, M.; Chassaing, T.; Hutter, J. Quickstep: Fast and Accurate Density Functional Calculations Using a Mixed Gaussian and Plane Waves Approach. *Comput. Phys. Commun.* **2005**, *167*, 103 – 128.

(34) VandeVondele, J.; Hutter, J. Gaussian Basis Sets for Accurate Calculations on Molecular Systems in Gas and Condensed Phases. *J. Chem. Phys.* **2007**, *127*, 114105.

(35) Goedecker, S.; Teter, M.; Hutter, J. Separable Dual-Space Gaussian Pseudopotentials. *Phys. Rev. B* **1996**, *54*, 1703–1710.

(36) Komsa, H.-P.; Rantala, T. T.; Pasquarello, A. Finite-Size Supercell Correction Schemes for Charged Defect Calculations. *Phys. Rev. B* **2012**, *86*, 045112.

(37) Wee, S.-H.; Kim, D.-W.; Yoo, S.-I. Microwave Dielectric Properties of Low-Fired $ZnNb_2O_6$ Ceramics with $BiVO_4$ Addition. *J. Am. Ceram. Soc.* **2004**, *87*, 871–874.

(38) Freysoldt, C.; Grabowski, B.; Hickel, T.; Neugebauer, J.; Kresse, G.; Janotti, A.; Van de Walle, C. G. First-Principles Calculations for Point Defects in Solids. *Rev. Mod. Phys.* **2014**, *86*, 253.

(39) Frenkel, D.; Smit, B. *Understanding Molecular Simulation: From Algorithms to Applications*; Academic Press: San Diego, CA, 2002.

(40) Ambrosio, F.; Wiktor, J.; De Angelis, F.; Pasquarello, A. Origin of Low Electron-Hole Recombination Rate in Metal Halide Perovskites. *Energy Environ. Sci.* **2017**, *11*, 101–105.

(41) Kirkwood, J. G. Statistical Mechanics of Fluid Mixtures. *J. Chem. Phys.* **1935**, *3*, 300–313.

(42) Liang, Y.; Tsubota, T.; Mooij, L. P.; Van de Krol, R. Highly Improved Quantum Efficiencies for Thin Film $BiVO_4$ Photoanodes. *J. Phys. Chem. C* **2011**, *115*, 17594–17598.

(43) Abdi, F. F.; van de Krol, R. Nature and Light Dependence of Bulk Recombination in Co-Pi-Catalyzed $BiVO_4$ Photoanodes. *J. Phys. Chem. C* **2012**, *116*, 9398–9404.

(44) Abdi, F. F.; Firet, N.; van de Krol, R. Efficient $BiVO_4$ Thin Film Photoanodes Modified with Cobalt Phosphate Catalyst and W-doping. *ChemCatChem* **2013**, *5*, 490–496.

(45) Cooper, J. K.; Gul, S.; Toma, F. M.; Chen, L.; Glans, P.-A.; Guo, J.; Ager, J. W.; Yano, J.; Sharp, I. D. Electronic Structure of Monoclinic $BiVO_4$. *Chem. Mater.* **2014**, *26*, 5365–5373.

(46) Ambrosio, F.; Wiktor, J.; Pasquarello, A. pH-dependent Surface Chemistry from First-Principles: Application to the $BiVO_4$(010)-Water Interface. *ACS Appl. Mater. Interfaces* **2018**, *10*, 10011–10021.

(47) Ambrosio, F.; Wiktor, J.; Pasquarello, A. pH-dependent Catalytic Reaction Pathway for Water Splitting at the $BiVO_4$-water Interface From the Band Alignment. *ACS Energy Lett.* **2018**, *3*, 829–834.

(48) Zachäus, C.; Abdi, F. F.; Peter, L. M.; Van De Krol, R. Photocurrent of $BiVO_4$ is Limited by Surface Recombination, not Surface Catalysis. *Chem. Sci.* **2017**, *8*, 3712–3719.

(49) Jo, W. J.; Kang, H. J.; Kong, K.-J.; Lee, Y. S.; Park, H.; Lee, Y.; Buonassisi, T.; Gleason, K. K.; Lee, J. S. Phase transition-induced Band Edge Engineering of $BiVO_4$ to Split Pure Water Under Visible Light. *Proc. Natl. Acad. Sci.* **2015**, *112*, 13774–13778.

(50) Liu, H.; Yuan, J.; Jiang, Z.; Shangguan, W.; Einaga, H.; Teraoka, Y. Novel Photocatalyst of V-Based Solid Solutions for Overall Water Splitting. *J. Mater. Chem.* **2011**, *21*, 16535–16543.